Figure S1

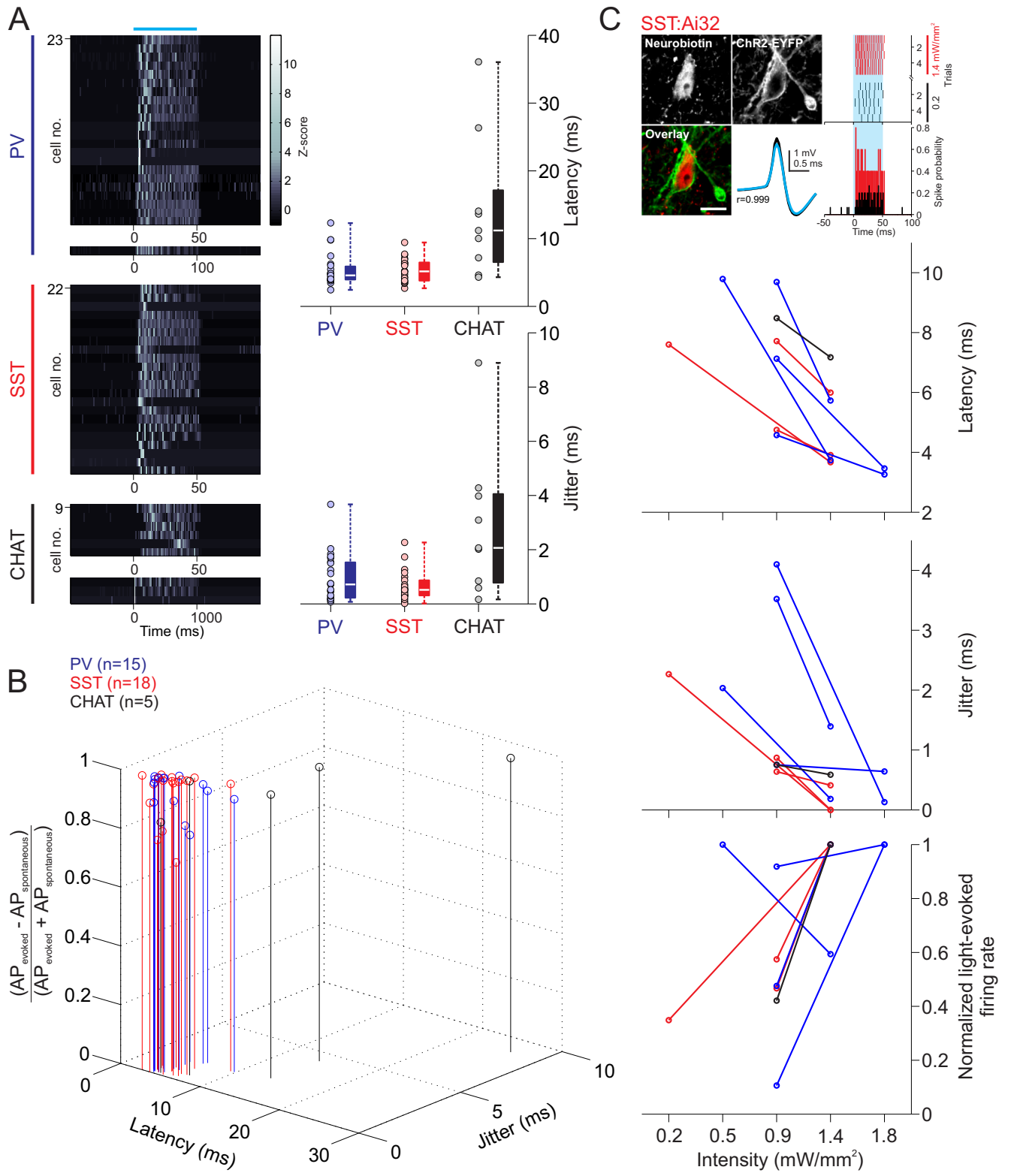
A
PV
SST
CHAT
cell no.
Z-score
Time (ms)
Latency (ms)
Jitter (ms)
B
PV (n=15)
SST (n=18)
CHAT (n=5)
Latency (ms)
Jitter (ms)
C
SST:Ai32
Neurobiotin
ChR2-EYFP
Overlay
r=0.999
1 mV
0.5 ms
Trials
Spike probability
Time (ms)
Latency (ms)
Jitter (ms)
Normalized light-evoked firing rate
Intensity (mW/mm²)

Figure S1, Related to Figure 2. Light activation parameters served to reliably identify ChR2-expressing cells. (A) Z-scored peristimulus histograms, latency and jitter to first spike of all cells recorded in the PV, SST and CHAT Cre driver lines (including data in Figure 2 and light responsive cells that were not histologically recovered and, thus, could not be verified as ChR2-expressing). Box plot central bar represents the median, and edges represent the 25^{th} and 75^{th} percentiles of the data set. Blue horizontal line represents light stimulus. (B) Light activation profile of all histologically ChR2-expressing cells exhibits characteristic identification parameters (i.e., short latency and jitter to first spike, and/or significant light-evoked activation). (C) Identification parameters increase with higher light intensities, aiding in the identification of ChR2-expressing cells. Top panel, representative example of histologically verified ChR2-expressing cell, its spontaneous (black) and light-evoked (light blue) spike waveforms, and light-evoked raster and peristimulus histogram for two light intensities (0.2 $mW \cdot mm^{-2}$ in black, and 1.4 $mW \cdot mm^{-2}$ in red). Blue shaded area represents light stimulus. Scale bar is 10 μm Second to fourth panels, latency, jitter to first spike and normalized light-evoked firing rate of identified cells in the PV (blue), SST (red), CHAT (black) Cre driver lines as a function of exposed light intensity at the tip of the pipette. Note that an expanded range is reported here as we attempted to characterize the temporal and magnitude aspects of light-evoked activity as a function of light intensity.

Figure S2

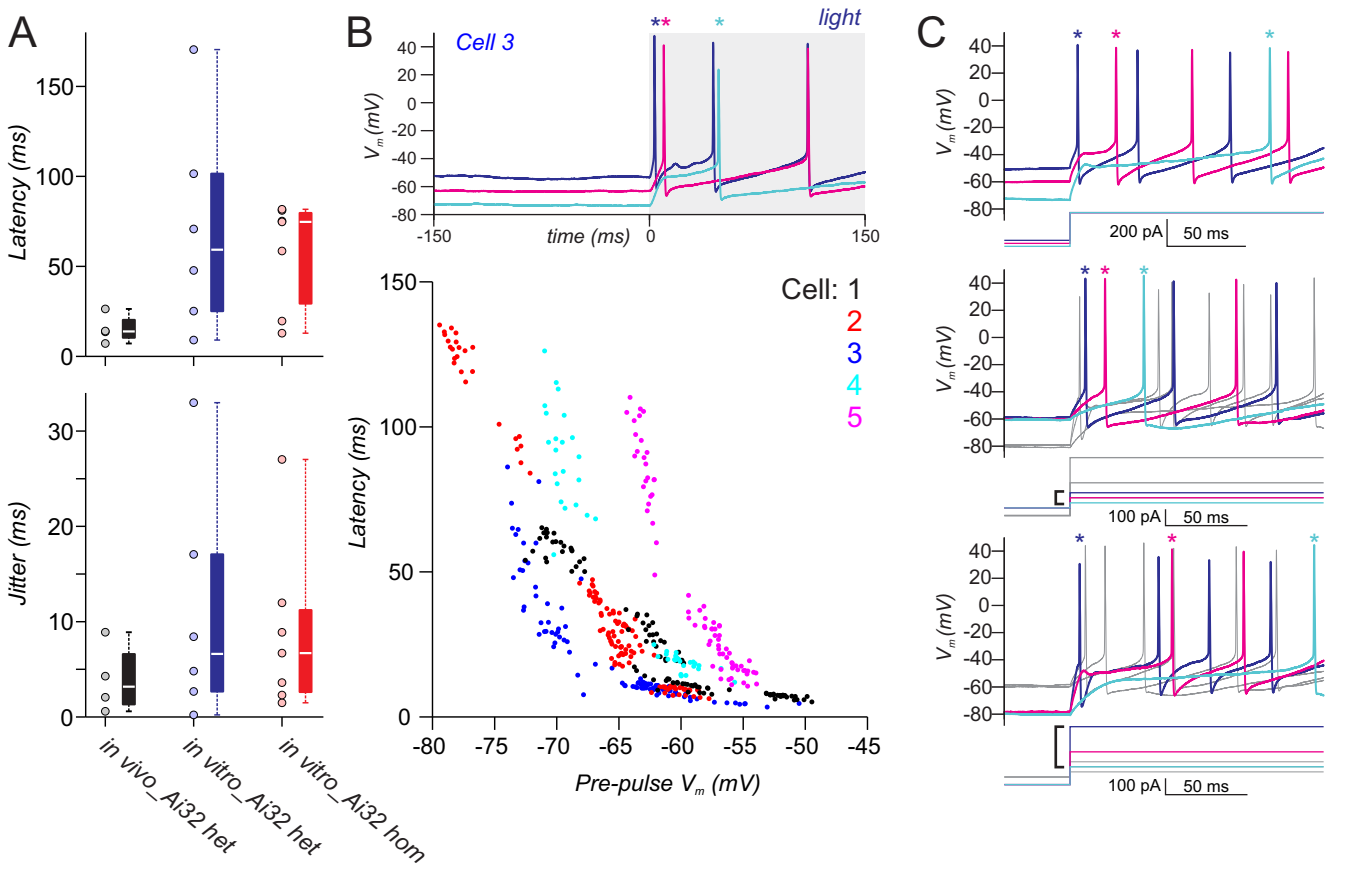

Figure S2, Relatedd to Figure 2. Membrane potential and biophysical properties account for variability in latency and jitter of light-evoked activity of basal forebrain cholinergic neurons. (A) Latency (top) and jitter (bottom) of first light-evoked spike of basal forebrain cholinergic neurons, recorded in loose-patch configuration *in vivo* (black, n = 4, same data as in Figure 2D), and *in vitro* from cells carrying one (blue, n = 5) or two (red, n = 7) copies of ChR2 transgene (i.e., heterozygous and homozygous Ai32 mice, respectively). (B) Latency of light-evoked activity of basal forebrain cholinergic cells recorded *in vitro* varies with membrane potential. Top, representative traces of light-evoked spike latencies at three different holding potentials (-53 mV, blue; -63 mV, magenta; and -73 mV, cyan) for basal forebrain ChR2-expressing cholinergic cell. Light-evoked spike latency (asterisks) decreases as the cell is held at more depolarized potential. Bottom, steep decrease in light-evoked spike latency with depolarized membrane potentials for ChR2-expressing cholinergic cells (n = 5) tested within a physiological range (-50 to -80 mV). (C) Top, similar dependency of current-evoked spike latency with membrane potential observed for a representative recording of a ChR2-expressing cholinergic cell. Note voltage hump after the onset of depolarizing pulse from a holding potential of -70 mV (cyan), suggesting the activation of a transient K^+ conductance. Middle and bottom, smaller intracellular current injections are required to evoke a short latency spike (<10 ms, compare black brackets on the side of current step protocols) from a representative ChR2-expressing cholinergic cell held above -60 mV (rheobase at 50pA, pale blue; short latency spike at 150 pA, dark blue) *versus* at more hyperpolarized membrane potentials (rheobase at 100 pA, light blue; short latency spike at 500 pA, dark blue).

Figure S3

PV:Ai32

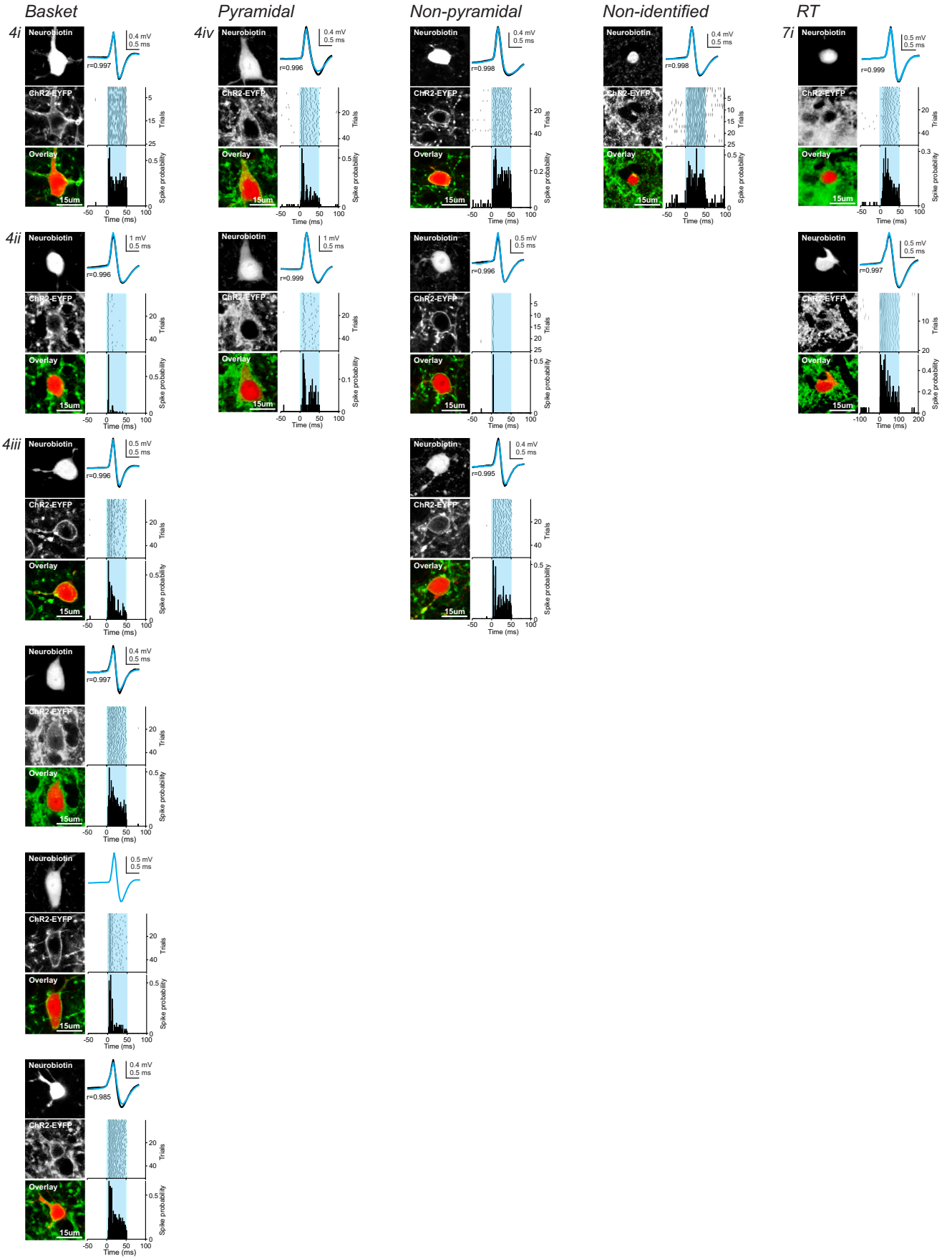

Figures S3, Related to Figure 4 and Figure 7. *Post hoc* histological verification of ChR2-EYFP expression in identified and recorded cells in the PV Cre driver line. Subpanels of recorded and labeled cells are arranged by morphological type (see text for definition). Code on the *left top* corner of certain subpanels is a reference to a main text figure showing the morphology of the cell. The code includes the figure and cell numbers (e.g., *4i* for cell *i* shown in Figure 4). For each subpanel, left, fluorescence and merged images of the neurobiotin staining and ChR2-EYFP expression of the recorded cell. Right top, spontaneous (black) and light-evoked (light blue) spike waveforms are highly correlated (Pearson correlation coefficient, $r > 0.98$). Raster (middle) and peristimulus histogram of spike probability (bottom) for multiple trials of light stimulation of the recorded cell. Blue shaded area represents light stimulus.

Figure S4

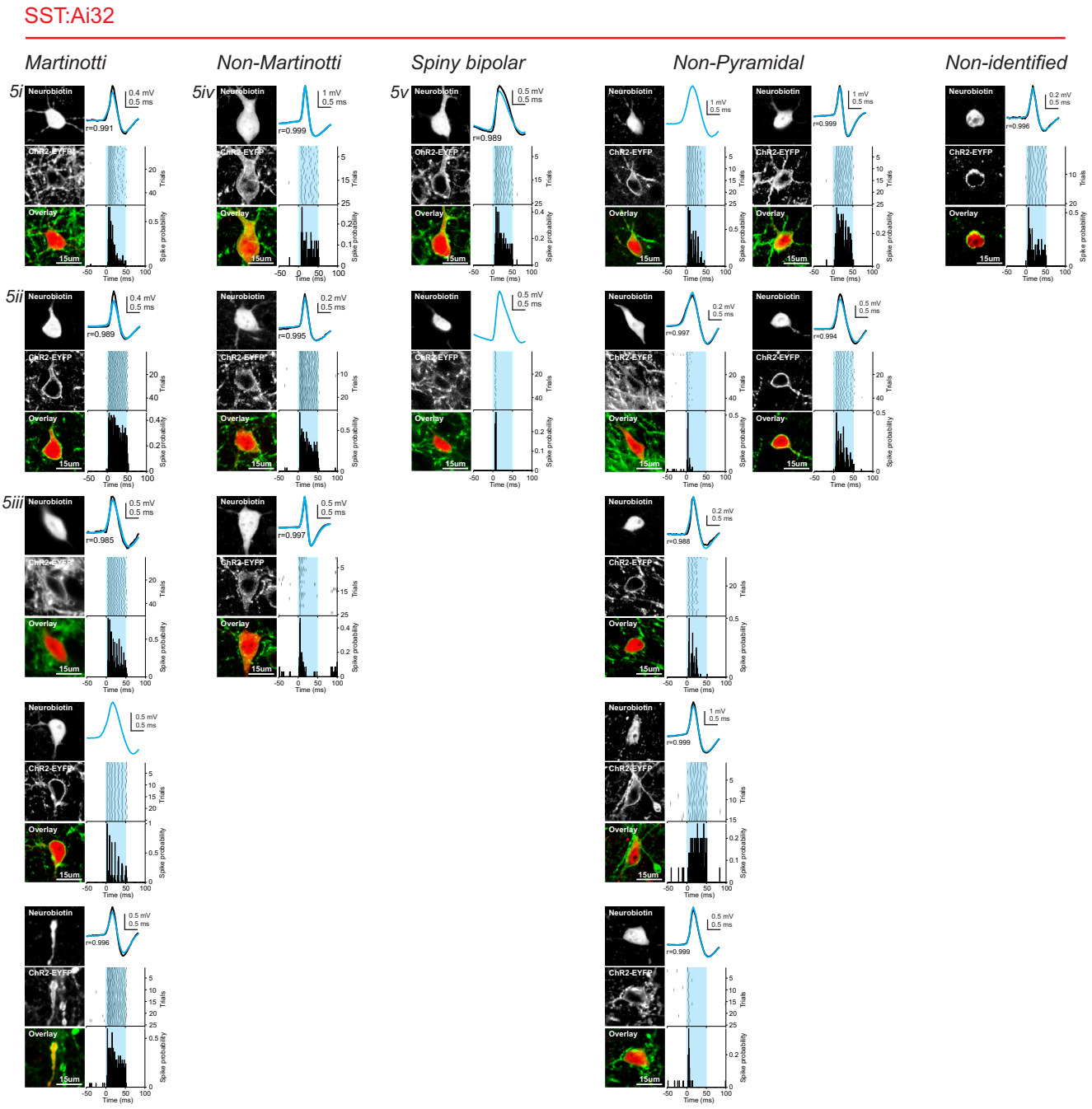

Figures S4, Related to Figure 5. *Post hoc* histological verification of ChR2-EYFP expression in identified and recorded cells in the SST Cre driver line. Subpanels of recorded and labeled cells are arranged by morphological type (see text for definition). Code on the *left top* corner of certain subpanels is a reference to a main text figure showing the morphology of the cell. The code includes the figure and cell numbers (e.g., *5i* for cell *i* shown in Figure 5). For each subpanel, left, fluorescence and merged images of the neurobiotin staining and ChR2-EYFP expression of the recorded cell. Right top, spontaneous (black) and light-evoked (light blue) spike waveforms are highly correlated (Pearson correlation coefficient, r > 0.98). Raster (middle) and peristimulus histogram of spike probability (bottom) for multiple trials of light stimulation of the recorded cell. Blue shaded area represents light stimulus.

Figure S5

CHAT:Ai32

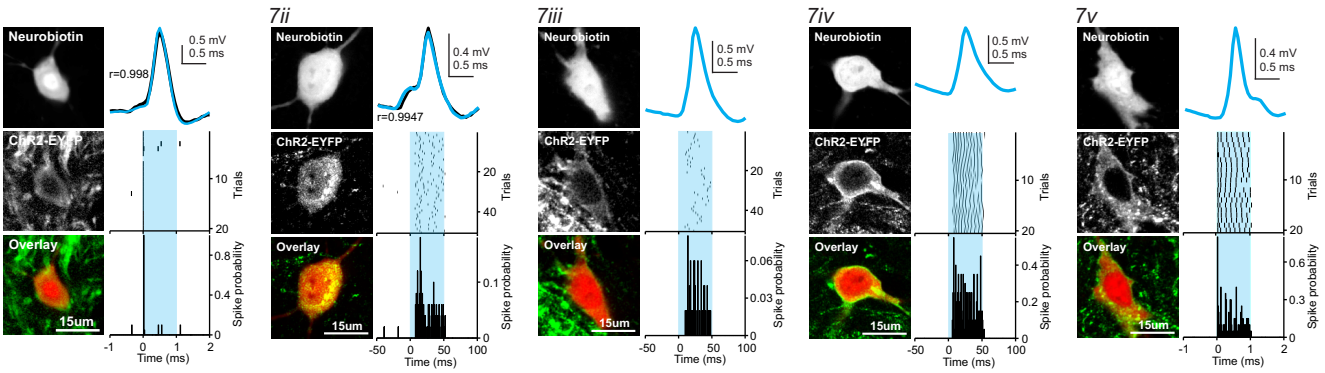

Figures S5, Related to Figure 7. *Post hoc* histological verification of ChR2-EYFP expression in identified and recorded cells in the CHAT Cre driver line. Subpanels of recorded and labeled cells are arranged by morphological type (see text for definition). Code on the *left top* corner of certain subpanels is a reference to a main text figure showing the morphology of the cell. The code includes the figure and cell numbers (e.g., *7ii* for cell *ii* shown in Figure 7). For each subpanel, left, fluorescence and merged images of the neurobiotin staining and ChR2-EYFP expression of the recorded cell. Right top, spontaneous (black) and light-evoked (light blue) spike waveforms are highly correlated (Pearson correlation coefficient, r > 0.98). Raster (middle) and peristimulus histogram of spike probability (bottom) for multiple trials of light stimulation of the recorded cell. Blue shaded area represents light stimulus.

Figure S6

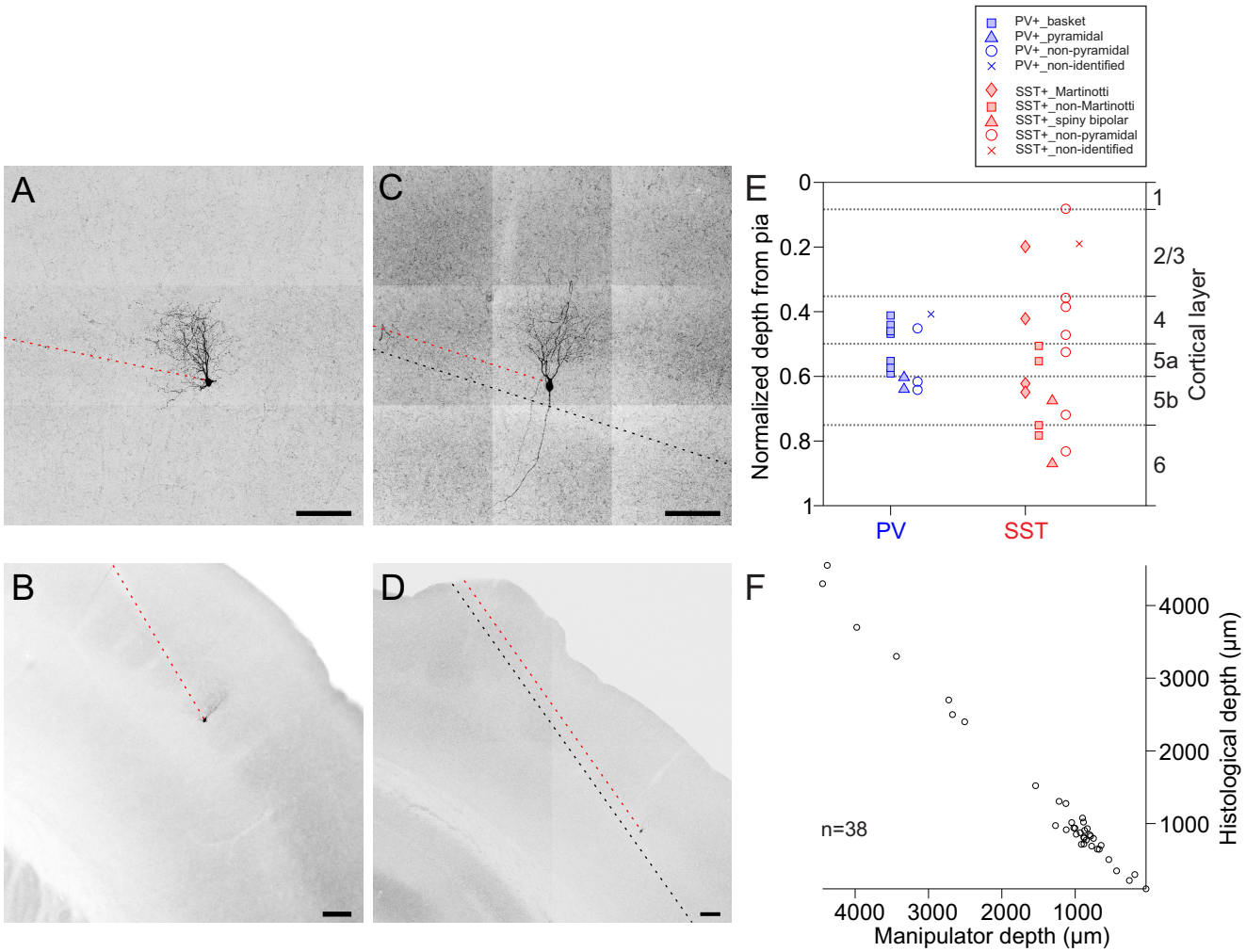

Figure S6, Related to Experimental Procedures: Histological recovery and position of *in vivo* juxtacellularly labeled neurons. (A-D) Quality of histological recovery of juxtacellularly recorded and labeled neurons. (A) High and (B) low magnification overview of a maximum intensity projection of a confocal image stack from neurobiotin-streptavidin Alexa 594 staining of a recovered ChR2-expressing PV cortical IN (Cell *i* in Figure 4), recorded and labeled *in vivo*. Section thickness: 100 µm. Only one ChR2-expressing neuron was recorded and filled in a particular area of the craniotomy and depth, in order to minimize ambiguity during *post hoc* identification of the multiple recorded and labeled cells in given animal. (C-D) Same for SST IN *iv* in Figure 5. Dashed lines indicate pipette tracks for the recorded neuron (red) or from other adjacent pipette penetrations that did not result in the encounter of a ChR2-expressing neuron (black). Note the absence of non-specifically labeled neurons along the pipette tracks. Scale bars are 100 µm. (E) Cortical depth and laminar position of recorded, labeled and morphologically identified PV- and SST-expressing cortical neurons. (F) Comparison of depth of the pipette tip measured with the micromanipulator versus depth measured histologically for recovered cells (n = 38).

Figure S7

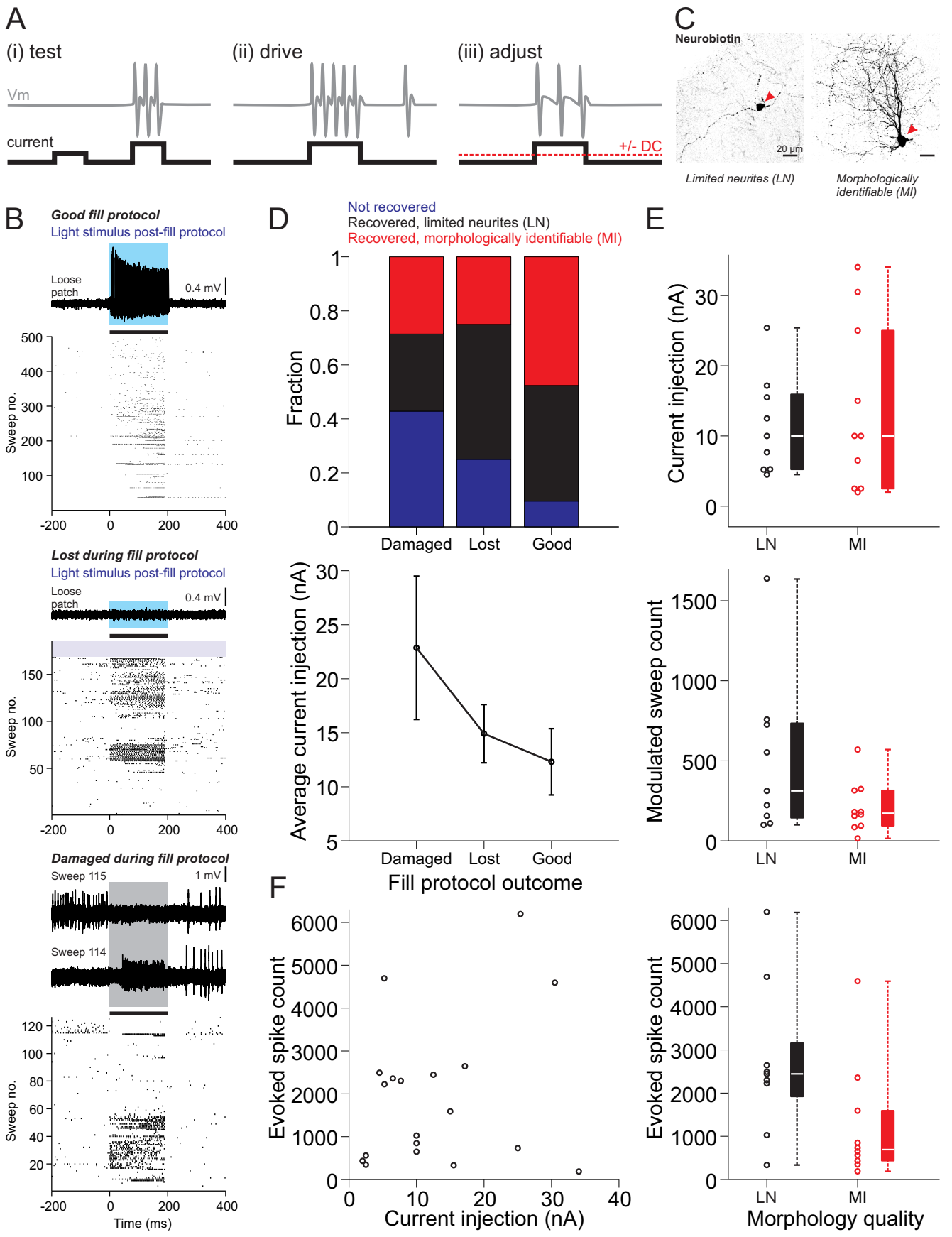
A
(i) test
(ii) drive
(iii) adjust
Vm
current
+/- DC
C
Neurobiotin
20 µm
Limited neurites (LN)
Morphologically identifiable (MI)
B
Good fill protocol
Light stimulus post-fill protocol
Loose patch
0.4 mV
Sweep no.
Lost during fill protocol
Light stimulus post-fill protocol
Loose patch
0.4 mV
Sweep no.
Damaged during fill protocol
Sweep 115
1 mV
Sweep 114
Sweep no.
Time (ms)
D
Not recovered
Recovered, limited neurites (LN)
Recovered, morphologically identifiable (MI)
Fraction
Damaged
Lost
Good
Average current injection (nA)
Damaged
Lost
Good
Fill protocol outcome
E
Current injection (nA)
LN
MI
Modulated sweep count
LN
MI
F
Evoked spike count
Current injection (nA)
Evoked spike count
LN
MI
Morphology quality

Figure S7, Related to Experimental Procedures. Optimizing parameters for the juxtacellular labeling of genetically defined cell types. (A) Strategy for the juxtacellular labeling of cortical interneurons showing: (i) current threshold search, (ii) driving current and (iii) adjustment of current-evoked firing rate (see Experimental Procedures). (B) Top, representative example of a *good* fill protocol outcome. In this case the protocol proceeds completely and uneventfully, as observed in the raster plot (black bar indicates current injection); light activation of the labeled cell is still observed at the end (top traces, blue shade is light stimulus). Middle, a cell is considered *lost* during the fill protocol, when there is complete interruption of spontaneous and current-evoked spiking (grey shade in raster) and light-evoked spiking (blue shades), without a distinctive cause. Bottom, a cell is considered *damaged* during the fill protocol if a dramatic increase in baseline firing rate is followed by losing of the cell and/or a drop in seal resistance. This can be observed in the raster plot and top sweeps 114 and 115 in which there is a sudden increase in baseline activity and action potentials of greater amplitude are observed, the current injection can no longer modulate the activity of the cell and the cell is eventually lost. (C) Representative examples of morphological grades of the labeled cells. Upon *post hoc* histological examination, cells are either not recovered (n = 7 out of 36), recovered with limited neurites (left, fluorescence image of neurobiotin staining, where only soma, few dendritic or axonal branches can be observed, insufficient for proper morphological identification, n = 15 out of 36), or recovered and morphologically identifiable (right, fluorescence image of neurobiotin staining, n = 14 out of 36). (D) Top, comparison of fill protocol outcomes with the morphological grade of the labeled cells shows that the fraction of recovered cells with limited neurites (black) and morphologically identifiable cells (red) is greater for the good fill protocols, while the fraction of not recovered cells (blue) is greater for the fill protocols during which cells were considered damaged. Bottom, good protocol outcomes can be maximized if the average current injection is kept low (12.3 ± 3.1 nA, mean ± SEM). (E) Comparison of *good* fill protocol parameters of recovered cells (n = 19) with limited neurites (black, n = 9) and morphologically identifiable cells (red, n = 10) shows that these only differed significantly in the total number of current-evoked spikes, suggesting that too much spike modulation can compromise post-fill cell viability. Only cells with *good* fill protocols are included in order to assess the parameters predicting the quality of morphological recovery. (F) The total number of current-evoked action potentials does not correlate with the average current injection amplitude, and, thus, it is of crucial importance to carefully monitoring how much the current steps drive the cell and adjusting it accordingly.

Supplemental experimental procedures

Surgery and training

For experiments under anesthesia, 1.5-2% isoflurane (Isothesia, Butler Schein Animal Health, vaporized in pure O_2 in Tec 7 vaporizer, GE Healthcare, at a flow rate 0.8-1 L/min) was employed and physiological body temperature (37°C) maintained with a temperature control module (FHC). After reflexes were suppressed, mice were placed in a stereotaxical frame (David Kopf Instruments), and metal bars for head fixation and a recording chamber were affixed on the skull of the animal with cyanoacrylate glue and dental cement (Metabond, Parkell). A craniotomy was drilled over brain areas for targeted recordings (from bregma: 1.2-1.5 mm posterior and 3.0-3.5 mm lateral for S1 cortex; 0.8-1.7 mm posterior and 1.5-2.5 mm lateral for thalamic reticular nucleus; 0.2–1.7 mm posterior and 1.5-4.5 mm lateral for striatum, nucleus basalis and zona incerta). Craniotomies were stabilized by applying a thin layer of 1.5% agar dissolved in NRR, and continuously irrigated with NRR. Importantly, a picture of the craniotomy and blood vessel pattern was taken with a camera connected to the surgery microscope to map the position of each electrode penetration and for morphological and anatomical analyses.

For recordings in awake, head-restrained conditions, mice were allowed a recovery period (2-3 days) following headpost implantation and progressively habituated to remain quiet while head-restrained (10-12 days). On the day of the experiment, mice were anesthetized and craniotomies were drilled and stabilized as above after which the recording chamber was filled with NRR and sealed with a coverslip and silicon elastomer (Kwik-Sil, World Precision Instruments) to keep the craniotomy intact during the recovery period. A picture of the craniotomy was taken and animals were returned to their home cage for recovery from anesthesia (2-3 hours), before the start of the recording session.

Viral injection of Thy1^{cre} mice

Thy1^{cre} mice were anesthetized and placed in the stereotaxical frame (as indicated above). A small burr hole was drilled, after which the injection glass pipette (o.d.: 10-20 µm) was inserted (from bregma: 1.2-1.5 mm posterior, 3.0-3.5 mm lateral, 0.6 and 0.9 mm ventral) and 50-100 nL of AAV1-EF1α-DIO-hChR2(H134R)-mCherry-WPRE-hGH (Penn Vector Core, University of Pennsylvania) were injected at a rate of 30 nL/min (Nanoject, Drummond Scientific). After the procedure, mice were sutured and allowed to recover and express viral vectors for 3-4 weeks before the recording session.

Sensory stimulation

For single whisker stimulation, whiskers were trimmed to a length of ~5 mm before recording. Individual whiskers were mechanically deflected using ceramic piezoelectric bimorphs (Piezo Systems) constructed according to (Simons, 1983). The piezoelectric bending actuator deflected principal whiskers in a ramp-and-hold fashion, at randomly interleaved onset-offset velocities (amplitude: 1.2 mm, direction: rostral and caudal, velocity: 26-187 mm/s). To smooth the corners of the driving waveform and avoid ringing of the piezoelectric device, we used a low-pass Bessel filter (8-pole) with -3 dB point of 100 Hz. Because of this smoothing, the velocities of the deflection were not constant. Here, we report the peak velocities reached during deflections. Deflections were delivered at ≤0.5 Hz to prevent steady-state adaptation of sensory-evoked activity. Multiple whisker stimulation was applied by a pressure system (Picospritzer III, Parker), which delivered 100 ms, 20 psi air puffs to the whisker pad, deflecting four to eight whiskers in two to three whisker rows by up to 2 mm.

Histology and cell reconstruction

At the end of the experiment, animals were given an overdose of anesthetic and fixed by transcardial perfusion with 0.9% saline, followed by a 4% paraformaldehyde, 15% v/v picric acid solution. The brain was extracted and 60-150 µm thick coronal sections were serially cut with a vibratome (VT100S, Leica). Floating sections were washed several times in sodium phosphate buffer (PB; 0.1 M Na_2HPO_4/NaH_2PO_4 aqueous buffer, pH 7.4) and incubated overnight in Alexa 488/594-conjugated streptavidin (1:500) solution made up in 0.1 M PB, containing 0.3% Triton X-100. Following several washes, sections were mounted on glass slides (Vectashield, Vector Laboratories). Confocal image stacks of labeled cells and their dendritic and axonal processes were acquired using a Zeiss LSM510 Meta confocal microscope with a 40X or 63X objective. Stacks were imported into Neurolucida software (MBF Bioscience) for digital reconstruction. Layers and barrels boundaries were determined using DAPI staining and were traced on every sections. Reconstructions were then rotated in x, y and z axes in order to orient the layers and pia as flat horizontal planes for side view visualization and this was rotated 90° for top view visualization. We did not apply any shrinkage correction. Despite the fact that we generally recorded many cells per craniotomy (up to 7), we could reliably assign labeled cells to their respective recordings because: (1) labeled neurons are the terminal point of a pipette tract, (2) labeled neurons match the tract position and depth of light-responsive cells and (3) labeled neurons express the ChR2-EYFP chimera.

Importantly, maintaining excessive positive pressure (>60 mbar) can lead to populations of nonspecifically labeled cells along the pipette tract, which represent a major issue for cell identification and reconstruction. However, in our experimental conditions (recording solution, neurobiotin concentration, searching pressure <40 mbar), we rarely encountered nonspecifically labeled cells compromising the identification and reconstruction of the recorded and filled cells. In fact, most nonspecifically labeled cells, when present, were very dim as compared to the filled cells and only their cell bodies were visible. In these cases, nonspecifically labeled cells can easily be ruled out because they do not meet the 3 criteria stated above.

Slice electrophysiology

Adult mice (2-6 months old) were given an overdose of anesthetic and upon loss of reflexes were transcardially perfused with ice-cold ACSF containing (in mM): 87 NaCl, 75 sucrose, 2.5 KCl, 1.25 NaH_2PO_4, 26 $NaHCO_3$, 10 glucose, 1 $CaCl_2$, 2 $MgCl_2$ (saturated with 95% O_2/5% CO_2). The animals were then decapitated, the brains quickly removed and immersed in ACSF. Coronal slices (300µm) were made using a Leica VT1200S vibratome and were incubated in a holding chamber at 36°C for 15 min and then at least 45 min at room temperature before electrophysiological recordings. During recording, slices were superfused with a solution containing (in mM): 125 NaCl, 26 $NaHCO_3$, 2.5 KCl, 1.25 NaH_2PO_4, 2 $CaCl_2$, 1 $MgCl_2$, and 10 glucose, saturated with gaseous carbogen (95% O_2/5% CO_2), in a chamber coupled to an upright BX50WI microscope (Olympus) equipped with infrared differential interference contrast and fluorescence illumination and filter cubes. ChR2-expressing neurons were selected for loose-patch recording or whole cell recording using similar glass electrodes and pipette solutions as for *in vivo* experiments for all recording configurations. Light stimulations were performed with the same configuration as for the *in vivo* experiments. Recordings were performed with an Axopatch 700B amplifier (Molecular Devices), low-pass filtered at 5kHz and sampled at 20kHz. For whole-cell recordings, cells with series resistance below 30MΩ upon break-in were used. Series resistance was fully compensated and data recorded were considered for analysis unless a significant change in series resistance was observed during the experiment (>20%). Membrane potential values are not corrected for liquid junction potential.

Supplemental references

Simons, D.J. (1983). Multi-whisker stimulation and its effects on vibrissa units in rat SmI barrel cortex. Brain research *276*, 178-182.